

Discovery of Extended X-ray Emission from the Planetary Nebula NGC 7027 by the Chandra X-ray Observatory

Joel H. Kastner

Chester F. Carlson Center for Imaging Science, Rochester Institute of Technology, 54 Lomb
Memorial Dr., Rochester, NY 14623; jhk@cis.rit.edu

Saeqa D. Vrtilek

Harvard-Smithsonian Center for Astrophysics, Cambridge, MA 02138; saku@cfa.harvard.edu

Noam Soker

Department of Physics, University of Haifa at Oranim, Oranim, Tivon 36006, ISRAEL;
soker@physics.technion.ac.il

Received _____; accepted _____

ABSTRACT

We report the discovery of X-ray emission from NGC 7027, a prototypical object for the study of the formation and evolution of planetary nebulae (PNe). Observations with the Advanced CCD Imaging Spectrometer (ACIS) aboard the Chandra X-ray Observatory show that the X-ray emission from NGC 7027 is extended and is bipolar in morphology. The ACIS spectrum displays strong emission from highly ionized Ne and weaker emission features which we attribute to O, Mg, and Si. Model fits to this spectrum suggest a characteristic temperature $T_x \sim 3 \times 10^6$ K and an intrinsic (unabsorbed) X-ray luminosity of $L_x \sim 1.3 \times 10^{32}$ ergs s $^{-1}$. The intranebular absorption of X-ray emission is highly nonuniform, but the modeling indicates an average column density $N_H \sim 6 \times 10^{21}$ cm $^{-2}$, consistent with previous measurements of relatively large visual extinction within the nebula. We suggest that the X-ray emission from NGC 7027 is or was generated by a hitherto undetected fast wind from the central star of NGC 7027, or from a companion to this star. Chandra's detection of extended, high-temperature X-ray emission from BD +30° 3639, NGC 6543, and now NGC 7027 suggests that such emission is a common feature of young planetary nebulae.

Subject headings: stars: mass loss — stars: winds, outflows — planetary nebulae: individual (NGC 7027) — X-rays: ISM

1. Introduction

The shaping of planetary nebulae (PNs) is a topic of considerable contemporary interest in astronomy (Kastner, Soker, & Rappaport 2000a). It has long been understood that a PN is the ejected envelope of an expired red giant star, which has been subsequently ionized and accelerated by the combination of UV radiation and fast winds from the emerging white dwarf that was the core of the former star. However, despite the appeal and widespread acceptance of the so-called “interacting winds” model of PN evolution (Kwok, Purton, & Fitzgerald 1978), crucial details of the morphologies and kinematics of many PNs do not appear to be explained by such a model (Frank 2000; Soker 2000).

The early stages of evolution of PNs (and/or proto-PNs) appear to hold the key to an understanding of the mechanisms ultimately responsible for shaping these objects (e.g., Sahai & Trauger 1998). The nearby (distance 880 ± 150 pc; Masson 1989), well-studied NGC 7027 represents a particularly intriguing and important object in this regard. It is evidently a young PN (dynamical age ~ 600 yr; Masson 1989) and displays a remarkably complex morphology. Optical imaging by the Hubble Space Telescope (Bond et al. 1997; Ciardullo et al. 1999) reveals a bright, compact ($\sim 5''$ radius) core region encircled by concentric rings of reflection nebulosity that extend to $15''$ in radius (Fig. 1a). The core region clearly suffers a large degree of spatially irregular (clumpy) extinction in the optical whereas, in the near-infrared (Kastner et al. 1994; Latter et al. 2000, hereafter L2000) and radio (Masson 1989), the ionized region is revealed to be an elliptical shell. Surrounding this shell, but largely interior to the system of concentric rings, is a photodissociation region with a remarkable cloverleaf or double-ring morphology that is best seen in near-infrared H₂ and PAH emission (Graham et al. 1993; Kastner et al. 1996; L2000).

Further complicating this picture is a system of at least two pairs of lobes protruding out from the main photodissociation region. L2000 speculate that these features, which can be seen both in H₂ emission and in reflection (Fig. 1a), are formed by fast, well-collimated outflows impinging on the relatively slowly expanding ($V_{\text{exp}} \sim 20$ km s⁻¹) shell of molecular gas surrounding the photodissociation region. If such fast, collimated flows are present, then wind interactions and/or

magnetic fields may be important in shaping this young PN (Blackman, Frank, & Welch 2000).

To investigate this possibility, we used the Chandra X-ray Observatory to observe NGC 7027, with the goal of detecting extended, high-temperature gas within this PN. According to theory (e.g., Mellema & Frank 1995; Soker 1994), very hot ($> 10^6$ K) gas is likely to be present if interacting winds or magnetic fields play an important role in sculpting a PN. Chandra imaging has already demonstrated the presence of an asymmetric “bubble” of hot ($\sim 3 \times 10^6$ K) gas in BD +30°3639 (Kastner et al. 2000b, hereafter KSVD) and an elongated “bubble” of X-ray emitting plasma in NGC 6543 (Chu et al. 2001). Whereas X-rays were detected from both BD +30°3639 and NGC 6543 prior to the Chandra observations of these nebulae, NGC 7027 had not been detected previously in X-ray emission. Given the many similarities between BD +30°3639 and NGC 7027, however, we anticipated that the latter also should be an X-ray source.

2. Observations and Data Reduction

Chandra observed NGC 7027, with ACIS as the focal plane instrument, on 2000 June 1. The duration of the observation was 18.2 ks. The Science Instrument Module was translated and the telescope was pointed such that the telescope boresight was positioned near the center of the spectroscopy CCD array (ACIS-S) and the coordinates of the PN fell on the central back-illuminated CCD (device S3). The ACIS-S3 pixel size is $0.49''$, similar to the spatial resolution of Chandra’s High Resolution Mirror Assembly. The Chandra X-ray Center (CXC) carried out standard pipeline processing on the raw ACIS event data, producing an aspect-corrected, bias-subtracted, graded, energy-calibrated event list, limited to grade 02346 events (ASCA system). From this list, we constructed a broad-band (0.3–10.0 keV) image. To improve its signal to noise ratio, the image was convolved with a Gaussian function with full-width at half maximum of 2.0 pixels, such that the resultant image (Fig. 1b) has an effective resolution of $\sim 1''$. *The image in Fig. 1b represents the first detection of X-rays from this well-studied PN.* The J2000 coordinates of the center of the X-ray nebula (as determined from the CXC-processed event list), RA = $21^h 07^m 01.75^s$, dec = $+42^\circ 14' 10.0''$ ($\pm 0.5''$), are the same, to within the uncertainties, as

the coordinates of the optical nebula (as listed in the SIMBAD¹ database).

We also extracted the ACIS pulse height spectrum of NGC 7027. To do so, we used CXC software to construct a histogram of pulse heights for events contained within a circle of radius 20 pixels ($\sim 10''$), an aperture judged to include all of the X-ray flux from NGC 7027. The broad-band (0.2–3 keV) ACIS-S3 count rate within this aperture was 0.014 counts sec^{-1} . The background count rate in a nearby, off-source region of equivalent area was ~ 0.001 counts sec^{-1} (0.2–3 keV). The ACIS-S3 count rate is consistent with the non-detection of NGC 7027 by ROSAT All-Sky Survey (RASS) observations in that, adopting a plausible X-ray emission model (§3.2), the ACIS count rate implies a ROSAT Position-Sensitive Proportional Counter (PSPC) count rate of $\sim 2 \times 10^{-3}$ counts sec^{-1} , well below the typical sensitivity limits of both the bright and faint source catalogs (Voges et al. 1999, 2000).

3. Discussion

3.1. X-ray Image

The Chandra image of NGC 7027 reveals that the nebula is clearly extended in X-rays, and shows a distinct butterfly morphology (Fig. 1b). While this morphology differs sharply from that of the clumpy, more or less elliptical nebula seen in the optical, the emitting region distributions correspond in several key respects (Fig. 1). First, the narrow “waist” just southeast of the center of the X-ray nebula — which appears to divide the nebula into a bright, northwest lobe and a fainter, southeast lobe — corresponds to a conspicuous “dark lane” located just southeast of the geometric center of the optical nebula. The optical dark lane marks the equatorial plane of the system or, perhaps, a ring of neutral material at high latitude (L2000) that is seen in absorption against the optical nebula. This “sense of perspective” is confirmed by the kinematics of molecular hydrogen emission from NGC 7027, which indicate that the NW side of the nebula is pointed toward the

¹<http://simbad.u-strasbg.fr/Simbad>

observer and the SE side is pointed away (L2000). Second, the brighter (NW) X-ray lobe is located on the side of the optical nebula that is closer to the observer. Third, the X-ray brightness peak located along the western edge of the NW lobe corresponds to the brightness peak of the optical nebulosity. Finally, the principal direction of alignment of the X-ray emission (NW-SE) follows that of projectile-like protrusions that appear in scattered light in the HST/WFPC2 color composite (Fig. 1a).

To illustrate better this last correspondence, we show in Fig. 2 an overlay of contours of X-ray emission on a near-infrared ($2.12 \mu\text{m}$) $\text{H}_2 + \text{continuum}$ image obtained by HST/NICMOS (L2000). The images have been registered such that the compact source of X-ray emission near the center of the Chandra image coincides with the position of the central star (see below). This registration requires the application of offsets of $+1.5''$, $+0.5''$ (in RA, Decl.) to the Chandra image, which are well within the absolute pointing uncertainties of Chandra. The overlay demonstrates that the X-ray emission is largely contained within the central, elliptical shell of bright nebulosity seen in the near-infrared. However, the brightest X-ray emission is detected along those directions extending from the central star toward the outermost H_2 filaments, especially along the direction toward the H_2 feature that extends $10''$ to the northwest of the central star (axis 1 in Fig. 3 of L2000).

The image overlay in Fig. 2 indicates the possible presence of X-ray emission from the vicinity of the central star. However, the image alignment in Fig. 2, while suggestive, is not unique and cannot be used to conclude that the central star is an X-ray source. Such emission, if present, is not nearly so prominent as in the case of the central star of NGC 6543 (Chu et al. 2001).

3.2. X-ray Spectroscopy

The Chandra pulse height spectrum of NGC 7027 shows that almost all detected photons have energies between ~ 0.2 keV and ~ 2.5 keV (Fig. 3). The spectrum, which peaks at ~ 1 keV, is evidently somewhat harder than that of BD $+30^\circ$ 3639, which peaks at ~ 0.5 keV (KSVD).

However, the spectra of both young PNs share a prominent feature at ~ 0.9 keV, which is likely due to a blend of Ne lines. The ACIS spectrum of NGC 7027 also displays weak features at ~ 0.6 keV, ~ 1.3 keV and ~ 1.8 keV, which we tentatively attribute to emission lines of O, Mg, and Si, respectively.

Guided by these identifications, we performed fits of a variable-abundance plasma emission model (the VMEKAL model) using the CXC’s Sherpa software (v1.1). The results, though highly uncertain due to the relatively small number of counts (~ 250) in the spectrum, indicate an approximate emitting region temperature $T_x \sim 3 \times 10^6$ K and volume emitting measure $\sim 2 \times 10^{54}$ cm $^{-3}$. The temperature is reasonably well constrained by the shape of the Ne feature, which suggests that emission from the Ne IX complex at 13.5 Å (0.89 keV) is stronger than that from the Ne X line at 12.1 Å (1.0 keV). The fit suggests the X-ray emitting region has near-solar abundances of O and Ne, and overabundances of He, C, N, Mg, and Si. As in the case of BD +30° 3639 (KSVD), no Fe emission is evident in the ACIS spectrum of NGC 7027.

The intervening absorbing column derived from the fitting is $N_H \sim 6 \times 10^{21}$ cm $^{-2}$, which is in good agreement with measurements of visual extinction within the nebula (e.g., $A_V = 2.97$ mag; Robberto et al. 1993). It is apparent, however, that the absorption is highly nonuniform. In Fig. 4 we present spectra extracted for 5'' \times 5'' square regions encompassing the NW and SE X-ray lobes of the nebula. The spectrum of the fainter SE lobe is evidently harder than that of its brighter NW counterpart, suggesting considerably larger intervening absorption toward the SE lobe. Thus, the above result for N_H represents the average absorbing column toward the dominant emission source, i.e., the NW lobe. Adopting the model results for mean N_H and for T_x , we derive a total observed flux of $F_x = 3.1 \times 10^{-14}$ ergs cm $^{-2}$ s $^{-1}$ and total unabsorbed (intrinsic) source luminosity of $L_x = 1.3 \times 10^{32}$ ergs s $^{-1}$.

4. Conclusions

The detection by Chandra of extended, high-temperature X-ray emission in the central regions of BD $+30^{\circ}$ 3639 (KSVD), NGC 6543 (Chu et al. 2001), and now NGC 7027 suggests that many or even most young planetary nebulae may harbor very high temperature inner regions. Such emitting regions, including that in NGC 7027, likely have escaped detection by previous X-ray telescopes due to a combination of their compact source sizes and obscuration along our lines of sight. Indeed, the values of T_x , emission measure, and L_x derived for NGC 7027 (§3.2) are very similar to those found for BD $+30^{\circ}$ 3639 (KSVD). Given this similarity, and the similar apparent X-ray emitting volumes of the two PNs, it is apparent that the large difference in their Chandra/ACIS-S count rates is due primarily to the larger absorbing column characterizing the emission from NGC 7027. Furthermore, the correspondence between the optical and X-ray morphologies of NGC 7027 (Fig. 1), and the sharp differences between the surface brightnesses and spectral energy distributions of the two X-ray lobes (Fig. 4), strongly suggests that the “patchy” X-ray appearance of NGC 7027 is determined in large part by foreground extinction in the nebula itself.

We conclude, therefore, that the same mechanism is responsible for the X-ray emission from both NGC 7027 and BD $+30^{\circ}$ 3639, and that the differences between their X-ray spectra and morphologies are largely a result of viewing angle. That is, the two nebulae have very similar intrinsic structures — prolate ellipsoidal shells with multiple protrusions along specific directions at high latitude — but BD $+30^{\circ}$ 3639 is viewed more nearly pole-on than NGC 7027. This interpretation is consistent with the measurement of large molecular outflow velocities in BD $+30^{\circ}$ 3639 (Bachiller et al. 2000) and with the smaller visual extinction measured toward its central star ($A_V \sim 0.75$ mag; Leuenhagen, Hamann, & Jeffery 1996).

It is very likely that the X-ray emission from both PNs originates in shocks formed by the collision of fast outflows from the central star(s) with slower-moving material within the elliptical shells detected in radio, infrared, and optical imaging. A similar mechanism likely explains the X-ray bubble that fills the central region of NGC 6543 (Chu et al. 2001). Both BD $+30^{\circ}$ 3639 and

NGC 6543 present evidence for fast winds, with velocities of $v_f = 700 \text{ km s}^{-1}$ (Leuenhagen et al. 1996) and $v_f = 1700 \text{ km s}^{-1}$ (Perinotto, Cerruti-Sola, & Lamers 1989), respectively; no such fast wind has been detected in NGC 7027. One prediction of the foregoing model, therefore, is that the central star of NGC 7027 — or a companion to this central star (Soker & Rappaport 2000 and references therein) — drives a fast wind. If this fast wind were highly collimated it would explain simultaneously the “patchy” X-ray emission morphology of the nebula as well as its outer loops of H₂ emission (L2000). For the X-ray emitting gas to be shocked to a temperature of $3 \times 10^6 \text{ K}$ the minimum preshock fast wind velocity would be $\sim 400 \text{ km s}^{-1}$.

The electron density n_e can be obtained from the emission measure $\text{EM} \equiv n_e n_p V_x \simeq 2 \times 10^{54} \text{ cm}^{-3}$, where n_p is the proton density and V_x the volume of the X-ray emitting gas. Assuming that the X-ray emitting gas occupies half the volume of the inner cavity (Kastner et al. 2001), we estimate $V_x = 10^{50} \text{ cm}^3$. This suggests an average electron density $n_e \simeq 150 \text{ cm}^{-3}$. The cooling time for gas at $3 \times 10^6 \text{ K}$ is then given by

$$t_{\text{cool}} \simeq 7000 \left(\frac{n_e}{150 \text{ cm}^{-3}} \right)^{-1} \text{ yr}, \quad (1)$$

which, given the derived electron density, is much longer than the dynamical age of the nebula ($\sim 600 \text{ yr}$; Masson 1989). So, if the present wind speed is well in excess of $\sim 400 \text{ km s}^{-1}$, as would be expected for the present central white dwarf (see below), this would suggest heat conduction along magnetic field lines and/or mixing of the fast wind with nebular material acts to moderate the temperature of the X-ray emitting region (KSVD and references therein; Chu et al. 2001). The total mass of hot ($T \sim 3 \times 10^6 \text{ K}$) gas implied by our observations and modeling, $\sim 10^{-5} M_\odot$, suggests a duration of only $\sim 100 \text{ yr}$ for the episode of mass loss via a fast wind — less than the dynamical age of the nebula — assuming a mass loss rate typical of the central stars of young PNs (i.e., $\sim 10^{-7} M_\odot \text{ yr}^{-1}$) and that the X-ray-emitting gas is dominated by fast wind (rather than nebular) material.

The presence of a luminous source of X-rays within NGC 7027 raises the intriguing possibility that this emission is ultimately responsible for the excitation of its infrared H₂ line emission (e.g., Gredel & Dalgarno 1995) and, perhaps, for the presence of certain key species in its molecular

envelope (e.g., HCO^+ ; Deguchi et al. 1990). In a subsequent paper (Kastner et al. 2001), we further pursue these and other suggestions raised in this paper and in KSVD.

The authors thank the referee, You-Hua Chu, for incisive, illuminating comments on this paper. J.H.K. acknowledges support for this research provided by NASA/Chandra grant GO0–1067X to RIT. N.S. thanks the US-Israel Binational Science Foundation. S.D.V. acknowledges support from NASA grant NAG5–6711.

REFERENCES

Bachiller, R., Forveille, T., Huggins, P. J., Cox, P., & Maillard, J. P. 2000, *A&A*, 353, L5

Blackman, E., Frank, A., & Welch, C. 2001, *ApJ*, 546, 288

Bond, H. E., Fullton, L. K., Schaefer, K. G., Ciardullo, R., & Sipior, M. 1997, in *IAU Symp. 180, Planetary Nebulae*, ed. H. J. Habing & H. J. G. L. M. Lamers (Dordrecht: Kluwer), 211

Ciardullo R., Bond H.E., Sipior M.S., Fullton L.K., Zhang C.-Y., & Schaefer K.G. 1999, *AJ*, 118, 488

Chu, Y.-H., Guerrero, M.A., Gruendl, R.A., Williams, R.M., & Kaler, J.B. 2001, *ApJL*, in press

Deguchi, S., Izumiura, H., Kaifu, N., Mao, X., Nguyen-Q-Rieu, Ukita, N. 1990, *ApJ*, 351, 522

Frank, A. 2000, in “Asymmetrical Planetary Nebulae II: From Origins to Microstructures,” eds. J.H. Kastner, N. Soker, & S. Rappaport, *ASP Conf. Ser.* Vol. 199, p. 225 (astro-ph/9912191)

Graham, J. R., Serabyn, E., Herbst, T. M., Matthews, K., Neugebauer, G., Soifer, B. T., Wilson, T. D., & Beckwith, S. 1993, *AJ*, 105, 250

Gredel, R., & Dalgarno, A. 1995, *ApJ*, 446, 852

Kastner, J. H., Gatley, I., Merrill, K. M., Probst, R., & Weintraub, D. A. 1994, *ApJ*, 421, 600

Kastner, J.H., Soker, N., & Rappaport, S., eds. 2000a, “Asymmetrical Planetary Nebulae II: From Origins to Microstructures,”, *ASP Conf. Ser.* Vol. 199

Kastner, J.H., Soker, N., Vrtilek, S.D., & Dgani, R. 2000b, *ApJL*, 545, L57 (KSVD)

Kastner, J.H., Soker, N., & Vrtilek, S.D. 2001, in preparation

Kastner, J. H., Weintraub, D. A., Gatley, I., Merrill, K. M., & Probst, R. 1996, *ApJ*, 462, 777

Kwok, S., Purton, C. R., & Fitzgerald, P. M. 1978, *ApJ*, 219, L125

Latter, W. B., Dayal, A., Bieging, J. H., Meakin, C., Hora, J. L., Kelly, D. M., Tielens, A. G. G. M. 2000, *ApJ*, 539, 783 (L2000)

Leuenhagen, U., Hamann, W.-R., & Jeffery, C. S. 1996, A&A, 312, 167

Masson, C. R. 1989, ApJ, 336, 294

Mellema, G. & Frank, A. 1995, MNRAS, 273, 401

Perinotto, M., Cerruti-Sola, M., Lamers, H.J.G.L.M. 1989, ApJ, 337, 382

Robberto, M., Clampin, M., Ligori, S., Paresce, F., & Staude, H. J. 1993, A&A, 280, 241

Sahai, R., & Trauger, J.T. 1998, AJ, 116, 1357

Soker, N. 1994, AJ, 107, 276.

Soker, N. 2000, in “Asymmetrical Planetary Nebulae II: From Origins to Microstructures,” eds. J.H. Kastner, N. Soker, & S. Rappaport, ASP Conf. Ser. Vol. 199, p. 71 (astro-ph/9909258)

Soker, N., & Rappaport, S. 2000, ApJ, 538, 241

Voges, W. et al. 1999, A&A, 349, 38

Voges, W. et al. 2000, <http://www.xray.mpe.mpg.de/rosat/survey/rass-fsc/>

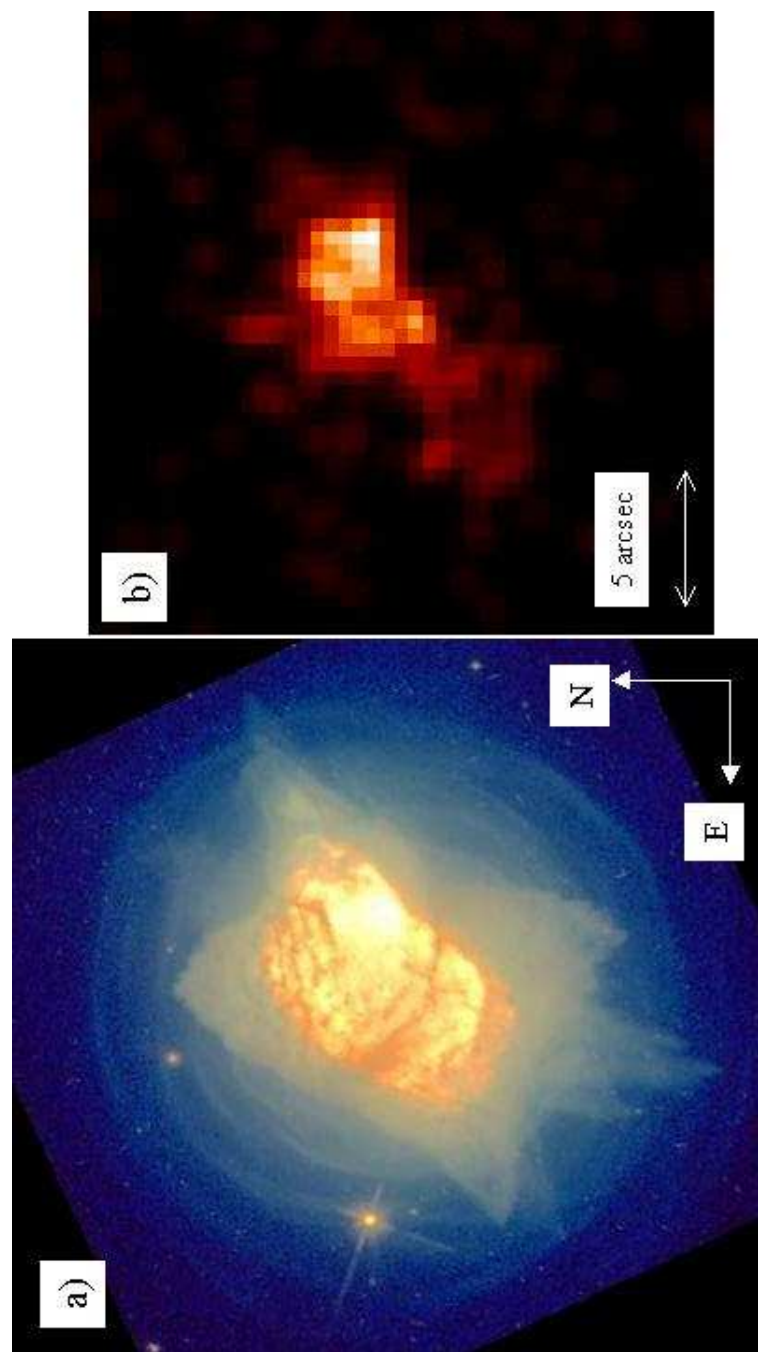
Figure Captions

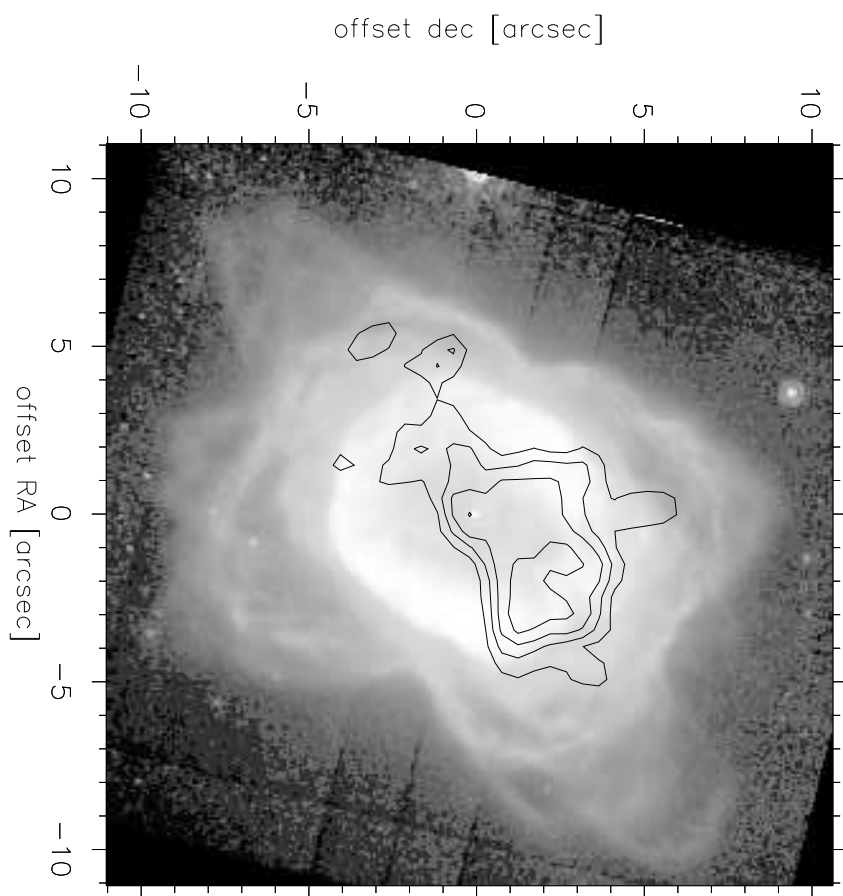
Figure 1. Comparison of *a*) Hubble Space Telescope (HST) optical (Ciardullo et al. 1999) and *b*) Chandra X-ray Observatory images of NGC 7027. The HST color composite was generated from images obtained through filters F555W (5550 Å) and F814W (8140 Å).

Figure 2. Overlay of Chandra X-ray Observatory image of NGC 7027 (contours; levels at 3, 5, 7, and 10 counts per pixel integrated over the 18.2 ksec observation) on a Hubble Space Telescope near-infrared image, obtained at 2.12 μ m (Latter et al. 2000). The HST image is dominated by H₂ rovibrational emission, but also includes contributions from continuum and He I emission.

Figure 3. *Top:* Chandra/ACIS spectrum of NGC 7027 (solid histogram), with “best-fit” model overlaid (dotted curve). The spectrum is presented for a bin size of 52 eV. *Bottom:* Residuals of the fit, in units of the measurement uncertainty for each spectral bin.

Figure 4. Comparison of spectra extracted for NW and SE X-ray lobes of NGC 7027. Both spectra are presented for a bin size of 52 eV.





NGC 7027: Chandra/ACIS spectrum

